Ocean Dynamics (2024) 74:251–265
https://doi.org/10.1007/s10236-024-01601-2

Observed seasonality of M2 and M4 tidal currents in the Gulf of Khambhat using high-frequency radars

Samiran Mandal[1]

Received: 31 August 2023 / Accepted: 24 January 2024 / Published online: 2 February 2024

Abstract
This study presents the initial findings from analyzing the ocean surface current observations during 2018 from the recently installed high-frequency (HF) radars in the Gulf of Khambhat in the northeastern Arabian Sea, India. The research is structured into two main sections: firstly, the extraction of the major (M2, S2, N2, K1, and O1) and shallow-water (M4, MS4, M6, and M8) tidal currents in the gulf, and secondly, understanding the impact of seasonal riverine freshwater influxes on the M2 tidal currents. The HF radars accurately captured strongest currents of ~2.0 m/s within the gulf. Additionally, the circulation pattern in the western gulf is mostly characterized by zonal currents, in contrast to the eastern gulf, where meridional currents prevail. Based on the findings of the higher harmonic analysis, it is apparent that the M2 tidal currents exhibit the highest magnitude, followed by other semi-daily constituents such as S2 and N2, as well as diurnal tidal constituents including K1 and O1. The M4 tidal currents, which are one of the shallow-water tidal components, exhibit strengths that span from 3.15 to 16.50 cm/s. The enhancement of tidal currents in the nearshore areas (within approximately 50 m) can be attributed to their interaction with the bottom bathymetry and the general coastline geometry of the gulf. Notably, higher values of Richardson number (R_i) and Brunt-Väisälä frequency (N^2) indicated the presence of highly stratified upper layers, particularly during September. The signatures of higher stratification during September contribute to the highest amplitude (>1.50 m/s) of M2 tidal currents.

Keywords Northeastern Arabian Sea · Gulf of Khambhat · Tidal currents · Shallow-water tides · Stratification

1 Introduction

The Gulf of Khambhat (GoKh), alternatively referred to as the Gulf of Cambay, is a bay with a distinctive trumpet-like shape bay situated on the western coastline of India. It is positioned between the Saurashtra Peninsula and the mainland of Gujarat, along the northeastern region of the Arabian Sea within India (Fig. 1a). The gulf is an inlet of the Arabian Sea (AS) and is named after the town of Khambhat (formerly known as Cambay) situated on its eastern shore. The GoKh has very shallow (<40 m) and complex bathymetry with strong tidal flats (Unnikrishnan et al. 1999a; Nayak and Shetye 2003; Sil et al. 2022). During the boreal summer, also known as the southwest monsoon season, significant river discharge is primarily attributed to major rivers such as the Narmada, Tapi, and Sabarmati. Moreover, the gulf has a rich mangrove ecosystem along the west coast, which makes the region well-adapted to several extreme oceanic conditions influenced by tides, waves, freshwater influxes, and the nature of substratum (Bhatt and Shah 2009; Ajai et al. 2013; Singh 2020). The GoKh exhibits a wide range of morphological characteristics, ecological attributes, and geological features, rendering it a subject of considerable interest for the investigation and comprehension of diverse coastal oceanic processes across different spatial and temporal scales. This knowledge is crucial for supporting various ongoing industrial activities such as navigation and the oil and gas industry, as well as proposed developmental projects including freshwater impoundment and the harnessing tidal and thermal energy, etc.

The gulf is one of the highly energetic macro-tidal regimes and is well-known for its tidal range, which is one of the highest in the world. The tidal phenomenon,

Responsible Editor: Fanghua Xu

✉ Samiran Mandal
mandals@cas.iitd.ac.in; samiranmandal7@gmail.com

[1] Centre for Atmospheric Sciences, Indian Institute of Technology Delhi, Hauz Khas, New Delhi 110016, India

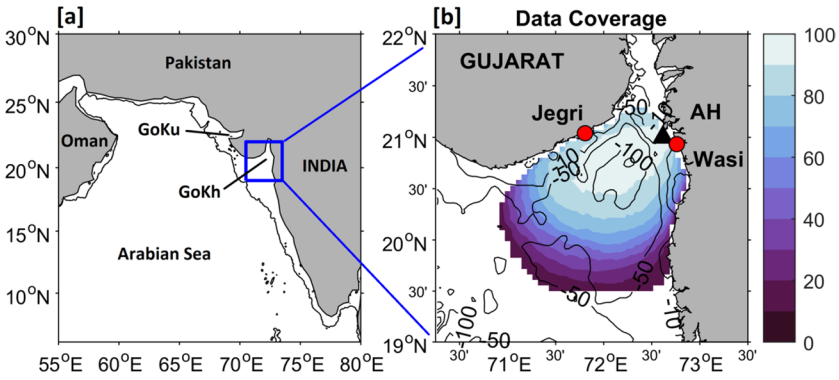

Fig. 1 **a** The study domain (blue box) with respect to the Arabian Sea. **b** Data coverage (shaded) in percentage (%) along the northeastern Arabian Sea during 2018. The red dots denote the HF radar stations at Jegri and Wasi. The black triangle indicates the tide gauge station at Adani Hazira (AH). The black contour indicates the −200 m isobath from ETOPO2

known as the "Khambhat" or "Cambay Tidal Bore" occurs when the incoming high tide forms a wave that travels upstream against the flow of rivers mostly attributed to the strong tidal flats (Nayak and Sahai 1985; Kumar and Balaji 2015). Earlier studies in the AS using the coarser resolution barotropic tidal models have shown the dominance of M2 tides, followed by K1, S2, O1, and N2 along the west (east) coast of India (Unnikrishnan et al. 1999b; Nayak et al. 2015; Testut and Unnikrishnan 2016). The western coast of India exhibits a varied tidal pattern, primarily characterized by semi-diurnal tides with an F-ratio ranging from 0.25 to 1.5. The GoKh also follows the same tidal regime (Nayak et al. 2015; Mandal et al. 2020a). The gulf has robust tidal currents that play a significant role in sediment transport together with their deposition, as well as contributing to coastal erosion within the region (Nayak and Sahai 1985; Unnikrishnan et al. 1999b; Kumar and Balaji 2015; Nayak et al. 2015; Testut and Unnikrishnan 2016; Mandal et al. 2020a). The tidal range can vary between 2 and 10 m, making it one of the highest tidal ranges (hyper-tidal) in the world. Using observed datasets from current profilers, Kumar and Kumar (2010) have conducted a study investigating the coastal ocean hydrodynamics inside the gulf, but for shorter time periods at a few locations outside and within the gulf. The tides in the gulf generate strong tidal currents that influence the movement of water. In recent times, Mandal et al. (2020a) have investigated the nature of flow-velocity tidal asymmetry in the GoKh using the higher-resolution high-frequency (HF) radar-derived surface currents during May 2012. Both studies have reported maximum flood and ebb currents within the range of 2.25–3.30 m/s of which flood currents have higher amplitudes (Kumar and Kumar 2010; Mandal et al. 2020a). The currents play a very crucial role in sediment transport and nutrient exchange within the region. Using the currents from location-specific acoustic Doppler current profilers (ADCP) off the gulf, characteristics of both the barotropic and baroclinic tidal currents have been quantified during different seasons off Jaigarh (Subeesh and Unnikrishnan 2016). The researchers have successfully evidenced internal tides within the shelf-slope regions within the vicinity of Jaigarh located on the central west coast of India. The Narmada, Tapi, Mahi, and Sabarmati are the key rivers, which contribute significantly to the freshwater runoff during the monsoon season. During the post-monsoon season, Rao et al. (2009) reported low salinity plumes off the gulf due to river discharges from multiple rivers, which remains trapped in the gulf until the withdrawal of monsoonal winds. These rivers discharge a lot of suspended silt (>1000 mg/L/day) leading to substantial sediment deposits in the GoKh. During monsoonal floods, the Narmada and Tapi rivers, which are the main rivers, discharge between 10,000 and 60,000 m^3/s. Also, a few studies have reported high tidal ranges and strong tidal current amplitudes in these regions, characterizing the domain as a hotspot for the extraction of tidal energy. This rapidly developing technology represents one of the highly efficient and potential sources of the marine renewable energy in the present time (Kumar and Balaji 2016).

All these earlier studies along the northeastern AS are either based on short-term observed datasets or coarser resolution numerical models, but reported about the wind-driven currents with preliminary insights into tidal currents and associated mixing within the continental shelf regions along the northeastern AS. Here are some key areas of research related to the GoKh:

1. Hydrodynamics: Understanding the tidal dynamics in terms of currents and sea level is very essential. Also, the presence of haline stratification modulates the internal tides and barotropic tidal currents within the continental shelf-slope zones, which can play crucial roles in controlling sediment transport and vertical mixing throughout the domain.
2. Sediment dynamics: It is very much needed to understand the sediment transport and deposition patterns in the gulf, coastal erosion, and shoreline changes to understand the geological evolution of the gulf.
3. Coastal processes and water quality: The surface circulation patterns, specifically the residual circulation pattern

can lead to complex mixing processes. Hence, efforts in assessing the water quality will help to understand water pollution and contamination studies within the gulf.

In recent times, five pairs of long-range HF radars (4.4 MHz) have been installed along the Indian coastline as part of the Indian Coastal Ocean Radar Network (ICORN) to monitor the coastal northern Indian ocean. These HF radars can cover ~200 km from the coastline and measure the surface currents every hour at ~6-km spatial resolution, which makes these datasets well-suited for observing coastal ocean surface circulation at comparable spatial and temporal scales (Fig. 1b). Based on the length of hourly data availability, the tidal currents have been mapped in many regions round the world, downstream of Hawaii (Chavanne et al. 2010), in Gulf of Farallones, California (Gough et al. 2010), in Monterey Bay (Paduan and Cook 1997; Rosenfeld et al., 2009), and along the northern Carolina shelf (Cook and Shay 2002), where researchers have investigated the role of complex bathymetry, seasonal stratification, surface winds, and mean circulation pattern on the tidal currents. Moreover, Kosro (2005) and Gough et al. (2010) have investigated the sub-tidal currents during the upwelling season using the HF radar surface currents off the Oregon coast and along the Gulf of Farallones, California. The HF radar surface currents datasets from the ICORN have been used at multiple spatio-temporal scales to understand the tidal current hydrodynamics (Mandal et al. 2018a; 2020b; 2021), to understand the evolution of mesoscale and sub-mesoscale lee eddies along the different coastlines (Arunraj et al. 2018; Mandal et al. 2019; 2022) and monitoring of the tropical cyclones (Mandal et al. 2018b).

The HF radar surface current observations are one of the first observations in the GoKh that can provide unpredicted insights into the spatial as well as temporal variability of the tides and associated dynamics within the gulf (Fig. 1b). The objective of this paper is to first validate these surface currents during different seasons and quantify the seasonal spatio-temporal variability of the major (M2, S2, N2, K1, and O1) and shallow-water (M4, MS4, M6, and M8) tidal currents in the GoKh. Further, the factors responsible for such seasonality will be investigated. The structure of this article is mentioned below. Section 2 provides a concise overview of the morphological and seasonal hydrodynamic characteristics of the study region, along with insights into the utilized datasets and adopted methodology. In Section 3, an in-depth examination of the validation and analysis of HF radar surface currents within the GoKh is presented. This analysis delves into the spatial and temporal fluctuations of significant (M2 and K1) and shallow-water (M4) tidal currents. The physical processes and dynamics involved in the dependence of these tidal currents on bathymetry and stratification are discussed in Section 4. Finally, the conclusions and the future scopes of this study are presented in Section 5.

2 Materials and methods

This section briefly describes the details of datasets used in this study with the specifications and technical description of the HF radar surface currents in Section 2.1 and other datasets in Section 2.2. The methodology adopted for this study with the analysis procedure is described in Section 2.3.

2.1 HF radar data

A network of five land-based, long-ranging (~4.45 MHz), and direction-finding HF radars (SeaSonde Systems) is operational in the northern Indian Ocean, which covers the western BoB, Andaman Sea, and GoKh (Jena et al., 2019; Mandal et al. 2018b). Specifically, a pair of these HF radars has been strategically positioned at Jegri and Wasi Borsi lighthouses on opposite sides of the gulf to monitor surface currents, with a typical range of approximately 200 km from the coastline (Fig. 1b). These HF radars are classified as direction-finding radars, which are equipped with both receiving and transmitting antennae. The antennae pattern type demonstrates an optimal configuration, exhibiting a threshold radial velocity of 2.55 m/s at both Jegri and Wasi Borsi locations. The HF radars are utilized to ascertain the velocity components near the surface in the radial direction, indicating movement either towards or away from the radar. These radial measurements are primarily derived from the motion of surface gravity waves that possess a wavelength approximately half that of the radar signal. After that, the least-squares fitting method is applied to these radial measurements taken from the two specific sites to estimate the total surface current vectors on a 6-km Cartesian grid. This fitting process is performed within a search radius of 10 km, limited to a specific region defined by the coordinates 19.40–22.70°N and 70.45–72.85°E. In order to uphold the integrity and quality of the obtained total surface currents, specific thresholds are implemented, which include a maximum total speed threshold and a maximum geometric dilution of precision (GDOP) threshold. The GDOP, acting as a scalar quantity, quantifies the influence of radial geometry on the level of uncertainty in velocity at a specific grid point.

Along the GoKh, the HF radars operate with a GDOP of 10, with the total velocity threshold capped at 2.50 m/s. These radars measure surface currents at a spatial resolution of approximately 6 km every hour and cover nearly 200 km from the coastline. It is emphasized that the hourly datasets undergo thorough quality assessment (QA) and quality control (QC) processes, following specific methods outlined in

the QA/QC manual, the details of which are also accessible at https://www.niot.res.in/documents/HFR_QAQC_doc.pdf. In addition, the configurations and specifications of the installed HF radar systems are listed in Table 1.

Although the range is approximately ~200 km, the data coverage may experience a decrease due to several factors, including diurnal ionospheric variations, atmospheric interferences, radio frequency interferences, and power-line disturbances (Rubio et al., 2017; Jena et al., 2019). Additionally, the coverage is diminished due to the removal of grid points over land and in close proximity to the coast, within a range of 1–2 km (Jena et al., 2019). It is important to note that the analysis conducted to quantify spatial variability was limited to HF radar grids that had a data coverage of more than 70% in terms of both space and time during January–December 2018. These higher-resolution hourly HF radar-observed surface currents, available at approximately 6-km intervals, are extensively utilized to examine the spatio-temporal characteristics of tidal currents during the pre-monsoon (April–May) and post-monsoon (September) seasons in 2018.

2.2 Other datasets

Owing to the absence of any other contemporary current dataset within the domain, the hourly sea-level anomaly obtained from a tide gauge located at Adani Hazira (AH) are extensively utilized concurrent with the duration of the HF radar surface currents (April–May 2018) are used for comparison and validation. The study utilized the daily ocean surface wind datasets, remotely sensed at 10 m by the Advanced Scatterometer (ASCAT), to examine the spatial distribution of seasonally varying winds in the GoKh in 2018. To gain insights into the salinity distribution in the gulf, the study utilizes remotely sensed sea surface salinity (SSS) datasets obtained from the Soil Moisture Active Passive (SMAP) satellite. These datasets are available monthly and provide information at a spatial resolution of 0.25° × 0.25°. Furthermore, the study analyzes the seasonal variability of temperature distribution in the GoKh using daily-gridded sea surface temperature (SST) datasets (1/12°) obtained from the Group for High-Resolution Sea Surface Temperature (GHRSST). The GoKh is a region with limited data availability, known for its shallow waters and prominent tidal flats. Since there were no other datasets containing information about the subsurface temperature and salinity, the study relied on monthly climatological datasets (1° × 1°) provided by the National Institute of Oceanography, India, to elucidate the seasonal variations in hydrography within the gulf (Chatterjee et al. 2012). This data has been used in many other studies. The climatological river discharge data for the major rivers (Narmada and Tapi) averaged over the 30 years are utilized to distinguish between seasons. Last but not the least, the study utilized the ETOPO2 bathymetry dataset, which provides information about the Earth's topography at a spatial resolution of approximately 3 km. This dataset was utilized to examine the dynamics that occur because of the interaction between tidal currents and the underwater topography.

Table 1 Specifications of the high-frequency (HF) radars in the Gulf of Khambhat (GoKh) along the northeastern Arabian Sea

Operating frequency	4.4 MHz
Signal form	Frequency modulated interrupted continuous wave (FMICW)
Duty cycle	50%
Band width	25 kHz
Radar wavelength (λ)	68 m
Ocean wavelength (Λ)	34 m
Ocean waveperiod (T)	4.66 s
Maximum range	200 km
Range resolution	6 km
Temporal resolution	1 hr

2.3 Methodology

The first step involves analyzing the spatial distribution of various physical parameters, such as SSS, SST, surface winds, sub-tidal currents, and river discharges, to characterize the gulf in terms of its hydrology. The sub-tidal currents are defined as the low-pass filtered currents at a cut-off frequency of 30 h, i.e., the high-frequency variations due to the semi-diurnal and diurnal tidal constituents have been excluded from the HF radar surface currents. Based on these physical characteristics, two seasons are identified to carry out the entire analysis. In 2018, during these distinct seasons, the hourly surface currents (both zonal and meridional components) are subjected to statistical analysis, specifically focusing on their standard deviation, to identify areas within the domain that exhibit higher variability. In order to conduct a more comprehensive analysis, a comparison is made between the surface currents obtained from HF radar and the sea-level anomaly data obtained from the tide gauge located at Adani Hazira over the period of April–May 2018. The basis for this comparison relies on the order of amplitudes of the tidal constituents derived from both the datasets by classical higher harmonic analysis, as outlined in Pawlowicz et al. (2002) and Mandal et al. (2018a). Subsequently, the spatio-temporal characteristics of the major (M2, S2, N2, K1, and O1) and shallow-water (M4, MS4, M6, and M8) tidal constituents are studied in this domain. Further, a detailed investigation is carried out to examine the seasonal variability of these major and shallow tidal constituents. Lastly, the reasons behind the seasonal variability of

tidal currents are studied, considering the interactions with bottom bathymetry and the impact of haline stratification resulting from freshwater influxes in terms of Brunt-Väisälä frequency (N^2) and Richardson's number (R_i). The N^2 and R_i have been calculated as:

$$N^2 = -\frac{g}{\rho}\frac{\partial \rho}{\partial z}$$

$$R_i = \frac{N^2}{(\partial u/\partial z)^2}$$

where "ρ" stands for density of seawater, "g" stands for acceleration due to gravity, "u" is the current speed, and "z" is the depth along the water column. In general, higher values of N^2 indicate higher stratification and highly stable water column. Moreover, R_i is a turbulence parameter that represents the balance between buoyancy-induced turbulence (N^2) and velocity shear-induced turbulence ($S^2 = (\partial u/\partial z)^2$). To interpret, whenever $R_i < 0.25$, the velocity shear overcomes the tendency of a stratified fluid to remain stratified, and some mixing happens. On the other hand, whenever R_i is on the higher end (>1), the turbulent mixing across the stratified layers is suppressed.

3 Results

This section discusses the study area in terms of hydrography and seasonal variability of the physical parameters in Section 3.1, followed by the statistical analysis of the hourly HF radar surface currents, comparison, and validation of these surface currents against the hourly sea levels in Section 3.2. The spatio-temporal variability of the major and shallow-water tidal currents is discussed in Section 3.3.

3.1 Geographical setting of study area

The GoKh is an important coastal region with unique morphology and hydrodynamics, which extends to 200 km (approx.) from its northernmost to the southernmost point (Fig. 1b). The gulf has a broad mouth that widens towards the south and opens into the AS. It is a relatively shallow domain, with an average depth ranging between 20 and 40 m. The bathymetry of the gulf is relatively flat and gently sloping seabed. Near the mouth of the gulf, the depth gradually increases as it transitions into the deeper AS. The GoKh is often considered an estuary, which is formed by the confluence of several rivers, most notably the Narmada and Tapi.

The GoKh experiences the influence of both tidal currents and wind-driven currents (Nayak et al. 2015; Mandal et al. 2020a; Sil et al. 2022). The wind-driven currents are affected by the monsoonal winds, where southwest winds dominate during the southwest monsoon and northeast winds prevail during the northeast monsoon. For this study, two specific seasons have been chosen: April–May (pre-monsoon season) and September (post-monsoon season). The hydrography of the northeastern AS shows significant seasonal variations of surface winds, SST, SSS, and sub-tidal currents as depicted in Fig. 2. Throughout both the seasons, the northeastern AS is primarily influenced by westerlies, with wind speeds ranging from 7.5 to 8.5 m/s in the pre-monsoon (April–May) and 5 to 6 m/s in the post-monsoon (September) (Fig. 2a and d). Comparing the pre-monsoon and post-monsoon seasons, the gulf exhibits higher SST and higher SSS during the pre-monsoon season, with gradients of approximately 1.5 °C and 1 psu, respectively (Fig. 2a–f). It is worth noting that the advection of colder waters from the south of Gujarat coast outside the gulf is consistently observed regardless of the season (Fig. 2a and d). The weak south-eastward sub-tidal currents (~11 cm/s) suffice this advection phenomenon, potentially driven by westerlies (Fig. 2c). In contrast, significant signatures of huge freshwater river influxes are observed during the post-monsoon season from the surface salinity maps, which are well supported by the strong sub-tidal currents (~26 cm/s) at the head and along the eastern gulf (Fig. 2e and f). Moreover, the climatological data on river influx from the two major rivers (Tapi and Narmada) in the GoKh indicate the highest (lowest) discharge occurring during August–September (March–April), which aligns with the spatial distribution of SSS and sub-tidal circulation pattern during the seasons (Fig. 2g). This results in strong density gradients signifying the prevailing influence of the buoyancy-driven currents during September. Thus, it can be concluded that the sub-tidal circulation pattern off the gulf is predominantly characterized by wind-driven currents, whereas the buoyancy-driven currents exert a strong influence along the head regions. The strong spatial gradients observed from the SST and SSS suggests that strong tidal mixing (either horizontal or vertical) could occur, and the associated tidal currents may significantly impact the coastline's formation and the transportation of sediment along the coast.

3.2 Quantification of tidal heights and tidal currents

The spatial maps of standard deviation of zonal and meridional components of the HF radar surface currents during the year 2018 are individually represented in Fig. 3a and b. It is interesting to note that the higher standard deviation is observed for either component, albeit limited to specific regions. In case of zonal currents, higher standard deviation values are observed along the western side of the GoKh, indicating increased variability and strengthened

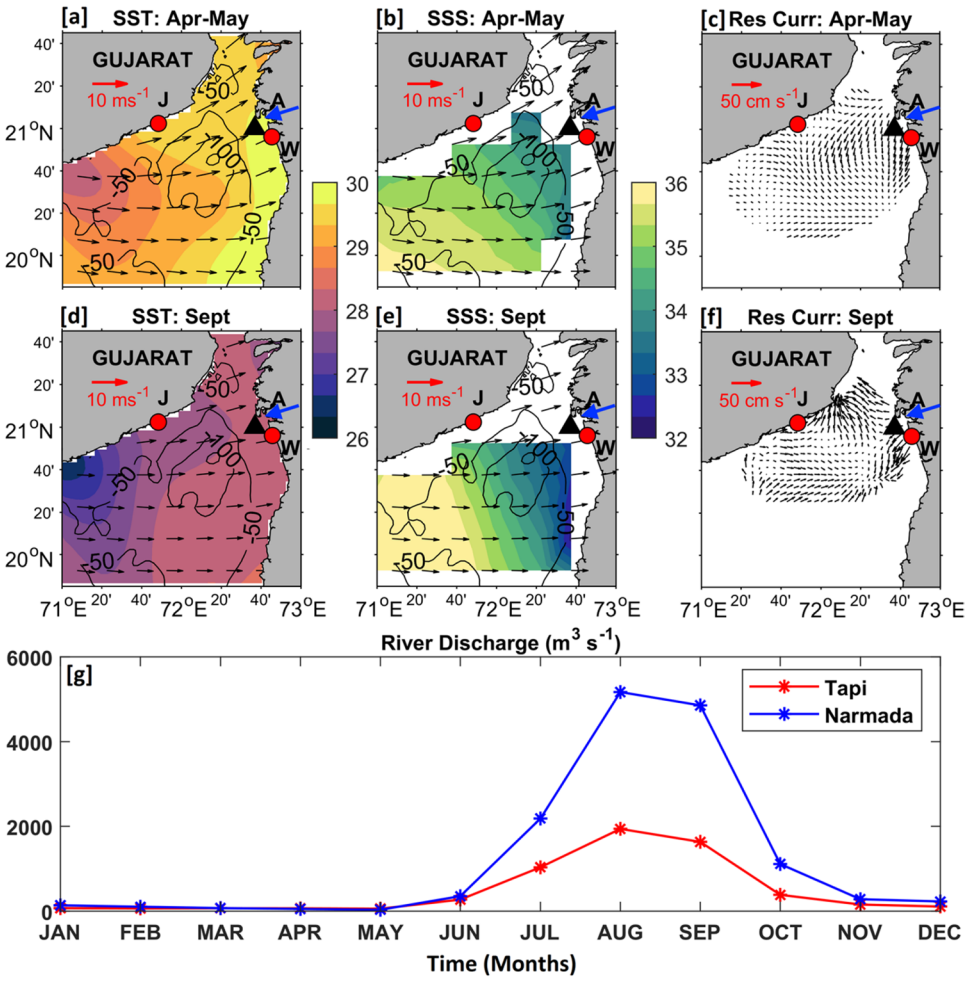

Fig. 2 The spatial distribution of sea surface temperature (SST, in °C), sea surface salinity (SSS, in psu) overlaid with wind vectors (black arrows), and subtidal currents (in cm/s) during **a**, **b**, and **c** April–May and **d**, **e**, and **f** September in 2018, respectively. **g** Climatological river discharges of two major rivers, namely, Tapi and Narmada, in the Gulf of Khambhat, Arabian Sea. The blue arrow indicates the freshwater discharge from the Tapi river. The red dots denote the HF radar stations at Jegri (J) and Wasi (W). The black triangle indicates the tide gauge station at Adani Hazira (A). The black contour indicates the −200 m isobath from ETOPO2

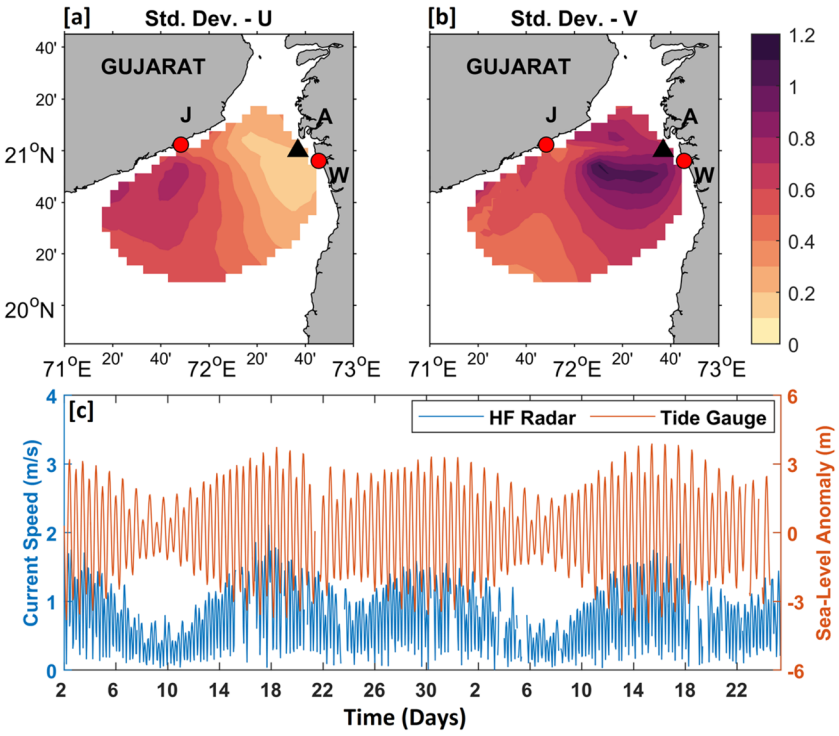

Fig. 3 The spatial maps of standard deviation of hourly **a** zonal currents (u-component) and **b** meridional currents (v-component) during 2018. **c** The temporal variability of HF radar-derived surface current speed (in m/s on the left y-axis) and sea-level anomaly (in m on the right y-axis) from the tide gauge at Adani Hazira (A) during April–May 2018

east-west movement of waters (Fig. 3a). On the other hand, significantly higher values are observed for the meridional component along the eastern side of gulf, which indicates prominent north-south movement of waters (Fig. 3b). It can be concluded that the meridional currents dominate most of the gulf, while a small area off Jegri is primarily influenced by the zonal currents, which can be attributed to the trumpet-shaped coastal geometry of the GoKh.

Due to the unavailability of any other surface current datasets (whether in situ or satellite-measured) in the domain, a comparison has been performed between surface currents derived from the HF radars and the tide gauge observed sea-level anomalies. Based on the data density and region of higher standard deviation, location "B" has been chosen near to the tide gauge station at AH for analysis (Fig. 3a, b). Also, two common periods during April–May and September in 2018 are chosen considering the minimal temporal gaps (Fig. 3c). During April–May, both the datasets indicate the occurrence of two spring-neap tidal cycles which coincide without any phase lag. The surface currents are observed to flow with a maximum speed of 2.11 m/s and attained maximum kinetic energy of 2.22 m^2/s^2 during the flood phase of a spring tide along with the highest tidal range of ~7.50 m. On the contrary, the least surface current speeds and least kinetic energies are observed during the neap phases of the tidal cycle, where the tidal range is also the least (Fig. 3c). It is interesting to note that the mean current speed and mean kinetic energy are 0.75 m/s and 0.37 m^2/s^2, respectively, indicating higher standard deviation in both the surface currents and sea-level anomaly (1.78 m), well supported by the standard deviation maps of zonal and meridional components of HF radar surface currents in Fig. 3a and b. For comparison and validation, the tidal constituent amplitudes have been quantified for both the datasets using the classical higher harmonic analysis technique. The amplitudes of the semi-major axes obtained from the surface currents are compared with those derived from the sea-level anomaly. This comparison is done individually for the major and shallow-water tidal constituents. The methodology followed here for comparison and validation is well established and justified in earlier studies (Mandal et al. 2018a; 2020a; Jena et al. 2020).

The tidal analysis of these two datasets suggests highest influence of the tidal constituent, M2, with maximum amplitudes of 110.03 cm/s and 226.91 cm for the surface currents (represented as u+iv) and sea-level anomaly, respectively (Fig. 4a). Except these, other notable semi-diurnal tidal constituents demonstrating considerable amplitudes are S2 (39.42 cm/s, 81.52 cm) and N2 (22.78 cm/s, 46.25 cm). The major diurnal tidal constituents are K1 (19.33 cm/s, 56.58 cm) and O1 (7.50 cm/s, 20.75 cm), respectively, for HF radar surface currents and sea-level anomaly at AH (Fig. 4a). Additionally, noteworthy amplitudes are noted for the shallow-water (M4: 4.73 cm/s and 13.08 cm) and fortnight (MSF: 3.35 cm/s and 1.63 cm) tidal constituents. The M2 tidal constituent prevails over other the tidal components. Here, the total tidal variance for HF radar surface currents (97.2%) is slightly lower than that of the sea-level anomaly data (99.5%).

The major tidal constituents (M2, S2, N2, K1, and O1) exhibit a higher correlation of 0.99 compared to the minor tidal constituents (MK3, SK3, M4, MS4, S4, 2MK5, 2SK5, 2MN6, M6, 2MS6, 2SM6, M8, and others) with a correlation coefficient (CC) of 0.90 (Fig. 4b and c). Similar results are observed in September, with M2 and S2 tidal constituents displaying the highest amplitudes. Additionally, notable correlations (CC > 0.85) are evident for these distinct set of tidal constituents in September (figure not shown). Table 2 presents the amplitudes of the semi-major and semi-minor axes for all tidal constituents observed throughout each of the time periods. The outcomes from higher harmonic analyses during these time periods have been collated in Table 2, prominently highlighting the prevalence of M2 and S2 tides.

Figure 4d–f provide insights into the total tidal variance and percentage variances specifically for the M2 and M4 tidal constituents. The range of tidal variance across the entire domain is between 20 and 95%, as depicted in Fig. 4d. Within this range, the southern side of 21°N, i.e., the mouth of the gulf, exhibits a significant prevalence of M2 tides, accounting to higher variance (70–85%) compared to the head region (10–50%) (Fig. 4e). Furthermore, it is worth noting that the M4 tides accounted for a significant portion, specifically 45%, of the overall tidal variance in the head region, as depicted in Fig. 4f. However, other factors, such as wind-driven currents, may also contribute to the overall tidal variance (Gough et al. 2010; Cosoli et al. 2013; Mandal et al. 2020b; Sil et al. 2022). Prominent signatures of tidal variance in the GoKh hint that the tidal currents, especially driven by M2 tides, play a significant role in driving the total surface currents within the gulf compared to the wind-driven currents. Depending on the tidal current amplitudes, M2 exhibits the highest amplitudes, followed by S2, N2, K1, and O1, indicating a semi-diurnal tidal regime in the domain (tidal form factor, F-ratio is 0.17 at location "B"). Furthermore, the spatial distribution of the F-ratio (less than 0.25) confirms the prevalence of a semi-diurnal tidal regime across the GoKh as a whole. In conclusion, the tidal constituents derived from HF radar surface currents at location "B" align well with those obtained from sea-level anomalies measured by the tide gauge at AH, both in terms of their order and amplitudes. It is worth noting that the amplitude of the semi-diurnal tidal currents, M2, exceeds those of K1 by more than fivefold.

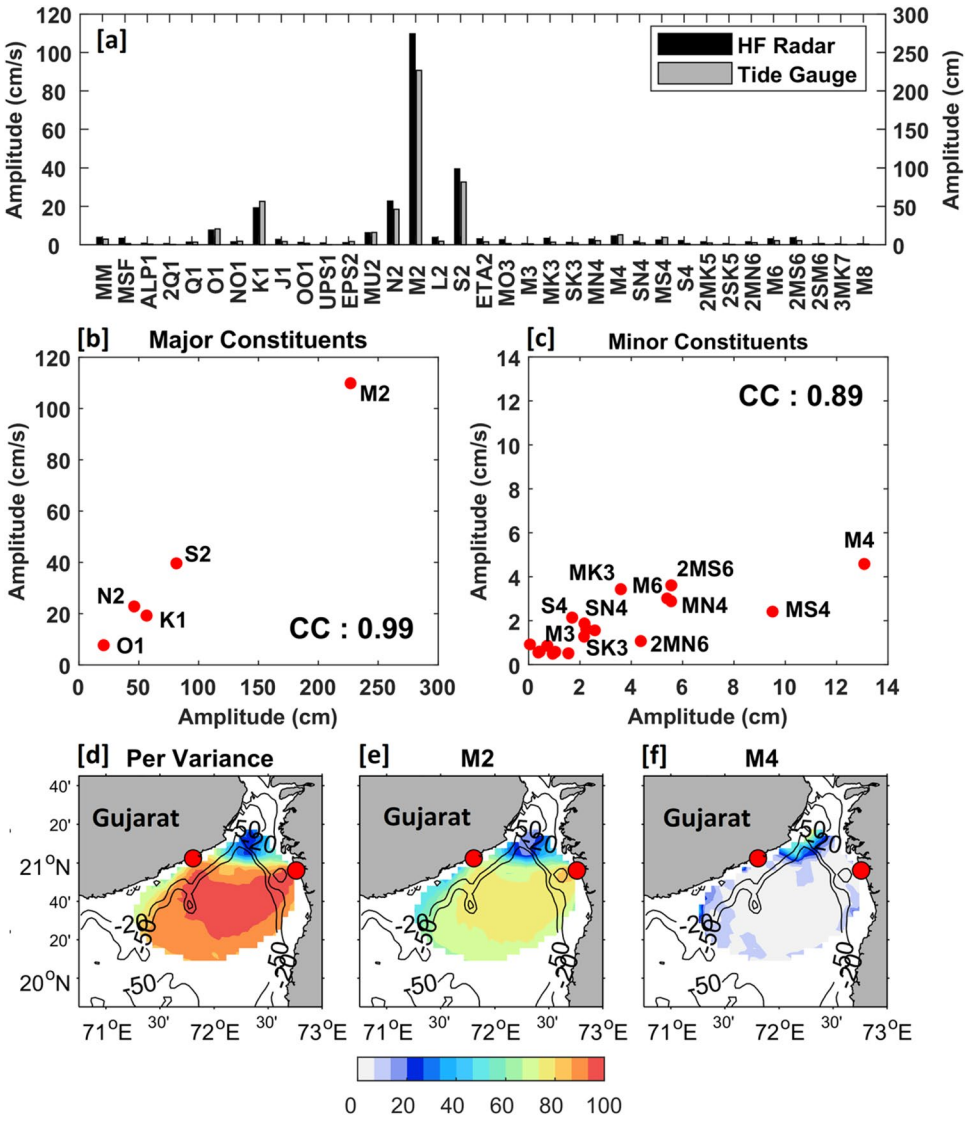

Fig. 4 **a** The amplitudes of semi-major axes corresponding to the tidal constituents derived from the HF radar surface currents (in cm/s) at point "B" and sea-level anomalies from tide gauge at Adani Hazira (in cm). The left (right) y-axis represents the black (gray) bars, which indicate the semi-major axes (tidal height) amplitudes from HF radars (tide gauge). The scatter plots for the comparison of the **b** major and **c** minor tidal constituents. **d** The spatial map of total tidal variance encompassing all tidal components (in %). The percentage tidal variance specifically attributed to the **e** M2 and **f** M4 tidal currents

Table 2 Amplitudes of semi-major axes (in cm/s), semi-minor axes (in cm/s), and tidal phase of the major and shallow-water tidal constituents from the HF radar currents at location "B" during April–May and September in 2018

Tidal const.	April–May			September		
	Semi-major (cm/s)	Semi-minor (cm/s)	Phase (°)	Semi-major (cm/s)	Semi-minor (cm/s)	Phase (°)
O1	7.50	−0.42	203.80	10.78	−2.54	131.41
K1	19.33	1.76	341.29	10.30	0.50	177.37
N2	22.78	3.30	296.40	34.93	2.93	60.58
M2	110.03	10.54	218.73	126.12	8.48	337.55
S2	39.42	4.78	262.35	52.11	6.74	209.68
M4	4.73	1.68	341.30	5.73	1.74	188.57
MS4	2.17	1.37	101.25	4.09	1.97	68.31
M6	2.82	0.26	159.31	2.73	0.19	157.14
M8	0.58	−0.02	253.22	1.39	−0.07	304.29

The constituents quantified in the table have signal-to-noise (SNR) ≥ 2

Negative minor axis means clockwise circulation

3.3 Seasonal variability of tidal currents

This portion emphasizes particularly on examining the temporal variation of major and shallow-water tidal currents in the gulf, which are quantified and extracted following the same higher harmonic analysis technique during April–May and September in 2018. The selection of these months was based on the seasonal changes of temperature and salinity patterns. Significant seasonal variabilities in both the major and shallow-water tidal constituents have been observed (Table 2). In September, the major semi-diurnal tidal constituents, M2 and S2, exhibited stronger amplitudes (with semi-major amplitudes of 126.12 cm/s and 52.11 cm/s) compared to April–May (with semi-major amplitudes of 110.03 cm/s and 39.42 cm/s). On the contrary, the tidal currents attributed to the major diurnal tidal constituent, K1, showed a significant decrease in September (10.30 cm/s) compared to 19.33 cm/s during April–May. In a comparable manner, the tidal constituents M4 and MS4 exhibited notable amplifications in the shallow-water region during the post-monsoon period in September.

Unlike earlier studies, the next section focuses on taking the advantage of higher-resolution (~6 km) HF radar surface currents to investigate and understand the spatial variability of the M2, K1, and M4 tidal ellipses in Section 3.4 during the above two seasons from HF radar datasets over a region of ~200 km from the coast.

3.4 Spatio-temporal variability of tidal currents

3.4.1 Variability of major tidal constituents (M2 and K1)

Tidal currents are commonly illustrated using a tidal ellipse, which captures the elliptical motion formed by vector components rotating in opposite directions and maintaining consistent amplitudes and phases. The interpretation of tidal ellipses typically relies on four important parameters: the semi-major axis, which denotes the direction of maximum current velocity, the semi-minor axes, the inclination angle, and the tidal phase angle indicating the phase lag (Prandle 1982; Maas and Van Haren 1987; Mandal et al 2020c).

Figure 5a and b depict the spatial maps of M2 tidal ellipses and tidal current amplitudes (semi-major axes) during the April–May and September in 2018. During the pre-monsoon period (April–May), substantial amplitudes of M2 tidal ellipses are detected, exhibiting anti-clockwise orientations that are prevalent across the whole domain (Fig. 5a). Nevertheless, a limited region in close proximity to the Jegri lighthouse has a prevalence of clockwise ellipses (Fig. 5a). It is important to understand that these observed M2 ellipses are almost rectilinear and in approximate alignment with the 20–50 m isobaths, so providing strong evidence flooding and ebbing of tidal currents. The uniformity of the orientation of these tidal ellipses within the continental shelf and slope areas across the entire region implies the presence of stronger surface currents influenced by M2 tides. Furthermore, the amplitudes of the M2 semi-major axes increase

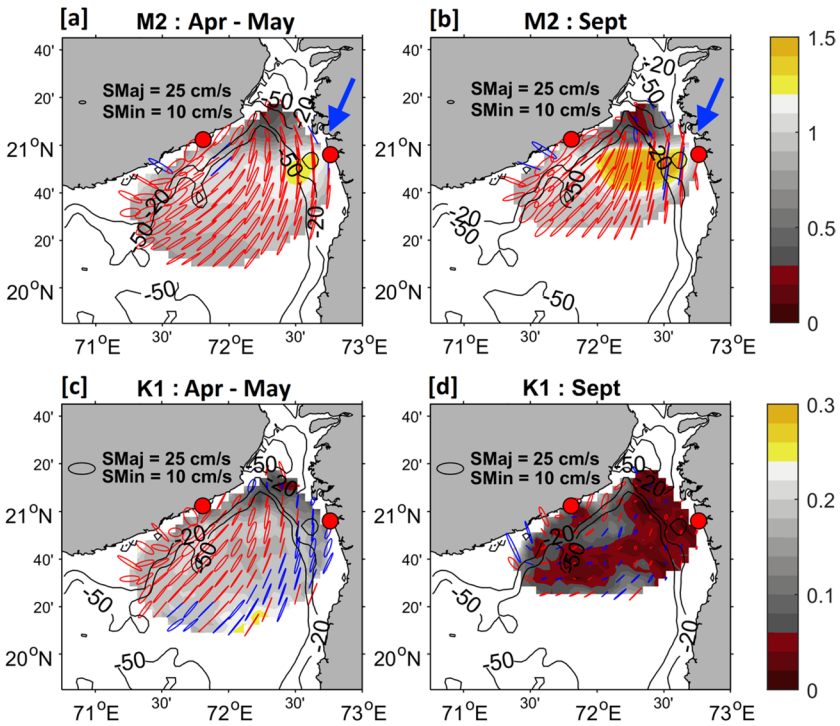

Fig. 5 The tidal ellipses associated to M2 (**a** and **b**) and K1 (**c** and **d**), as observed from the HF radar surface currents. The semi-major axes of the tidal ellipses are represented by the shaded background (in m/s), while the black contours illustrate the isobaths at −20 m and −50 m depths. The blue ellipses indicate clockwise rotation, while the red ellipses represent anti-clockwise rotation. The blue arrow indicates the freshwater discharge from the Tapi river

from the open ocean until 21°N and subsequently decrease towards the head, well supported by tidal variance maps in Fig. 4e. Notably, the highest M2 tidal current amplitudes, reaching nearly 1.32 m/s, are observed near the Wasi area. Interestingly, the same M2 tidal currents are observed to intensify significantly during the post-monsoon season in September (Fig. 5b). These tidal currents exhibit amplitudes exceeding 1.54 m/s near Wasi and cover a larger area. However, the intensities are approximately 0.30 m/s at the head of the gulf. The orientation of the M2 tidal ellipses during September is almost identical to that observed during April–May.

The diurnal tidal constituent, K1, in the gulf also exhibits pronounced seasonality (Fig. 5c and d). In April–May, the corresponding tidal ellipses are almost rectilinear and parallel to the −20 m and −50 m isobaths, like the observed pattern for M2. However, the K1-driven tidal currents (semi-major axes) have considerably smaller amplitudes compared to M2, ranging between 5.20 and 21.78 cm/s. Notably, a significant decrease of tidal current amplitudes is observed near the head gulf (Fig. 5c). Furthermore, the orientation of the K1 tidal ellipses significantly varies on either side of the gulf, i.e., a band of highly concentrated clockwise ellipses dominate the eastern GoKh, while the western part is characterized by anti-clockwise ellipses. On the other hand, in September, the spatial distribution of K1 ellipses is more variable in terms of both tidal current amplitudes and their orientation (Fig. 5d). A substantial reduction in the K1 tidal current amplitudes is evident, with the semi-major axis mostly varying between 2.10 and 10.78 cm/s throughout the domain, except a few patches on the western gulf. The M2 tidal currents exhibit a clear dominance and are nearly 4.5 times greater than the diurnal constituents across the whole domain in terms of amplitudes.

3.4.2 Variability of shallow-water tidal constituent (M4)

Tides are essentially long waves that originate in the open ocean and eventually reach shallow waters like continental shelves, bays, and estuaries. These tidal waves undergo modulation and distortion due to various hydrodynamic factors (mainly the bathymetry and channel geometry), resulting in the formation of shallow-water tidal constituents. These aforementioned aspects exert an influence on the tidal waves, resulting in modulations of both the amplitude and phase of these astronomical tidal constituents. Consequently, this leads to fluctuations in the tidal ranges as well. Simultaneously, multiple sub-harmonics are generated, which are known as overtides (M4, S4, M6, etc.) or compound tides (MK3, MS4, 2MS6, etc.). Understanding the shallow-water tides holds significant importance in the assessment of influence of tides and tidal currents on various coastal ocean phenomena. Despite this significance, there is a huge lacuna of studies round the world coasts on the shallow-water tidal constituents, which could be mainly attributed to their significant presence with minor amplitudes compared to other dominating ones and the prominent hydrodynamic forcings.

In the GoKh, multiple shallow-water tidal constituents (M4, MS4, M6, M8, etc.) are identified with significant amplitudes extensively utilizing the higher-resolution HF radar surface currents as well as the sea level anomalies from the tide gauge at AH. This section primarily emphasizes the spatial variability of the most dominant shallow-water tidal constituent, M4 (>12 cm/s) during April–May and September in 2018 (Fig. 6). The tidal ellipses are slightly more intensified in September than March–April in the gulf. However, irrespective of the seasons, extremely dense anti-clockwise tidal ellipses are observed across the domain except a few small patches of clockwise ellipses in the nearshore regions (i.e., within −50 m isobath) and head gulf (Fig. 6a and b). Moreover, the ellipses within the −50 m isobath are more intensified comparable to those near the mouth of the gulf. In terms of the amplitudes of these tidal currents, a gradual increase of the semi-major axes of M4 tides is observed from the offshore (1.65–4.66 cm/s) to the head gulf and shallow-water regions (7.64–20.54 cm/s), clearly indicating a notable rise in the amplitudes of tidal current amplitudes (Fig. 6c and d). A track has been chosen across the domain to examine the role of bathymetry on the M4 tidal current amplitudes, i.e., the fractional relationship between the semi-major axes and bottom bathymetry along the trajectory from south to north (indicated in Fig. 6e). The ratio clearly indicates linearity in the offshore regions (beyond −50 m isobath), whereas the non-linearity increases significantly within the shallower regions (i.e., at depths less than −50 m). These M4 tidal currents have the most the significant intensifications in the proximity to the gulf's head, where the corresponding amplitudes are almost half of those for M2 tides.

4 Discussion

First results on the seasonal variability of M2 tidal currents have been reported in this paper from the available higher-resolution (~6 km) and higher-frequency (hourly) HF radar surface currents in the GoKh. The M2 tidal currents are stronger (>1.53 m/s) during September and comparatively weak during April–May (1.25 m/s). This section discusses the fundamental results and henceforth the dynamics of the GoKh.

The spatial maps of ratio of M2 semi-major axes to bottom bathymetry and along the two transects are shown in the top panel of Fig. 7 (Fig. 7a, b). Along the transect to the western gulf (dotted line), the ratio shows significantly higher values within the nearshore regions (bathymetry

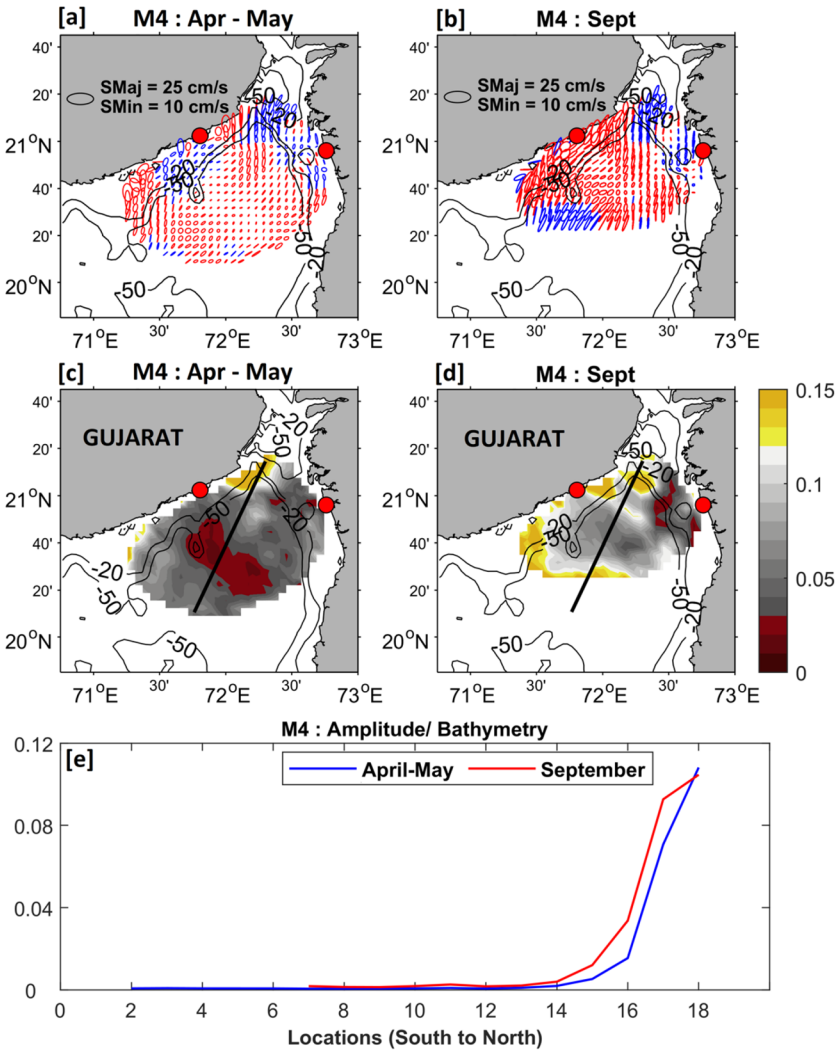

Fig. 6 The M4 tidal ellipses during **a** April–May and **b** September, as observed from the HF radar surface currents. The corresponding semi-major axes are shaded in **c** and **d**, respectively. The black contours denote the isobaths at −20 m and −50 m depths. The blue ellipses indicate clockwise rotation, while the red ellipses represent anti-clockwise rotation. **e** The ratio of semi-major axes and bathymetry during the two seasons along 72.25°N

more than −50 m), indicating strong non-linear tidal interactions irrespective of the seasons along the western and eastern gulf (Fig. 7c). On the contrary, the variations are almost negligible along the transect towards the head gulf (solid line), indicating reduced interaction between M2 tidal currents and bathymetry at the head gulf. It can be concluded that bathymetry plays a significant role in the intensification of M2 tidal currents along the western and eastern coasts, and the same is responsible for the intensification of M4 tidal currents at the head gulf.

Secondly, a significant amplification of the M2 tidal currents is observed during the post-monsoon season in the gulf. The temperature and salinity profiles show that the upper layers (10–20 m) have strong stratification, with higher values of Brunt-Väisälä frequency (N^2) and well supported by post-monsoonal strong riverine freshwater influxes (Fig. 7d). Moreover, this season also sees a shallow mixed layer depth (~7 m) implying less mixing. Since prominent signatures of both stratification and less mixing are noted in the gulf, so, the variations in Richardson number (R_i) are examined (Table 3).

In the gulf region, changes in the behavior of M2 tidal currents occur notably within the pycnocline due to water column stabilization in a stratified ocean environment. The typically higher eddy viscosity observed during the well-mixed conditions experiences a decrease as water column becomes more stratified. This increasing stratification enhances the stability of the water column, leading to the suppression of vertical mixing and consequently reducing the eddy viscosity within the pycnocline. This phenomenon, as documented by Maas and Van Haren (1987), Visser et al. (1994), Souza and Simpson (1996), and Müller et al. (2014), results in a diminished dissipation of tidal kinetic energy into turbulent ocean processes during September. Furthermore, a higher R_i (1.62) is evident in September compared to April–May (0.03), indicating constrained vertical mixing across the highly stratified layers, also indicated by Turner (1973). This phenomenon

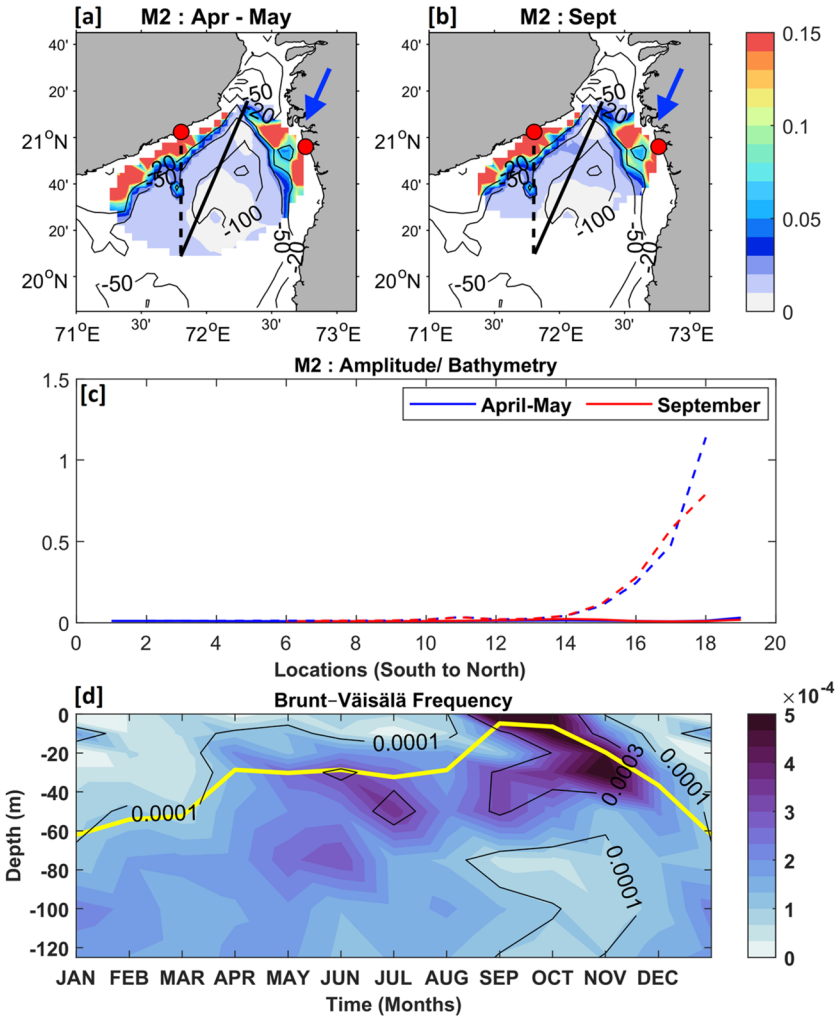

Fig. 7 The ratio of semi-major axes of M2 tidal constituent to bottom bathymetry in **a** April–May and **b** September in 2018. The blue arrow indicates the freshwater discharge from the Tapi river. **c** Along-track variation (as indicated in the top row) of the ratio of M2 tidal current amplitudes to bottom bathymetry during April–May (in blue) and September (in red). **d** The time-depth variation of climatological Brunt-Väisälä frequency (N^2) with the yellow-contoured mixed layer depth (in m) in the Gulf of Khambhat (GoKh), India

Table 3 Variation of the ocean physical and dynamical parameters with tidal currents

	Mixed ocean (April–May)	Stratified ocean (September)
Stratification (N^2)	Low (1.49×10^{-5})	High (80.45×10^{-5})
MLD (m)	~30 m	~5 m
Eddy viscosity	High	Low
Loss due to turbulence	Increased	Reduced
Tidal current (cm/s)	Low (2.5–5)	High (>6.5)

results in limited vertical displacements within the depths of the pycnocline, resulting in the separation of surface and subsurface strata. Consequently, the presence of such dissociated layers lowers down the friction between these layers. In simpler terms, increased stratification will ultimately decrease the eddy viscosity in the vicinity of the pycnocline, leading to an inhibition of turbulence within and thereby impeding the energy exchange. As a result, the M2 tidal current amplitudes with higher amplitudes are noticeable in September. In contrast, April–May experience well-mixed conditions with a deeper mixed layer (~30 m) and lower values of both N^2 and R_i (Fig. 7d). In these well-mixed conditions, the stabilizing effect exerted on these M2 tidal currents is inconsequential besides insignificant, resulting in a significantly less manifestation of surface tides due to the greater dissipation of energy in turbulent phenomena (Table 3).

It can be concluded that both bathymetry and stratification are major reasons for significant spatio-temporal variations in the M2 and M4 tidal currents. The higher amplitudes of the M2 tidal currents during September in the gulf can be attributed to the higher stratification due to the post-monsoonal freshwater influxes.

5 Conclusions

This study investigates the spatio-temporal variability of M2 and M4 tidal currents using the first surface current observations from the HF radars installed along the GoKh during pre-monsoon (April–May) and post-monsoon (September) seasons in 2018. The main results are as follows:

- The gulf experiences seasonal variability of temperature, salinity, and sub-tidal currents, with higher (lower) temperature and salinity conditions, well supported by minimum (maximum) freshwater river influxes during the pre-monsoon (post-monsoon) season in 2018.
- The findings from the statistical analysis of the HF radar surface currents indicate that zonal currents prevail on the western side of the gulf's mouth, whereas meridional currents dominate the eastern region of the gulf.
- The comparison of HF radar surface currents with sea level anomaly from tide gauge at Adani Hazira (in terms of amplitude and order) revealed that major tidal constituent, M2, is followed by S2, N2, K1, and O1 during both the seasons. The M2 tidal currents are nearly 5 times the amplitudes of the diurnal constituents. Among the shallow-water tidal constituents, M4 and MS4 are dominant ones in the shallow-water regions.
- The gulf is dominated by tidal currents with total variance of 95% throughout the domain, of which M2 tidal currents has variance of 70–85% except at the head, where the M4 tidal currents dominate with a variance of nearly 45%.
- The bathymetry of nearshore locations exerts a substantial influence on the strengthening of semi-diurnal and shallow-water tidal currents with the exception being observed near the head, where the tidal currents undergo rapid distortions due to the dominance of M4 tidal current amplitudes, irrespective of any season.
- The M2 tidal currents have the highest amplitudes (>1.53 m/s) during September in comparison to 1.25 m/s during April–May. The primary cause of the interseasonal variability in M2 tidal currents can be attributed to the significant perturbation occurring at the subsurface. This perturbation is primarily influenced by the higher stability of the water column during September, resulting in increased stratification, as well as lower levels of eddy viscosity. The inherent stability of this system results in a decrease in the dissipation of tidal kinetic energy, leading to the notable amplification of M2 tidal currents throughout the month of September.

To conclude, this article is a humble submission to investigate the higher-resolution (~6 km) and higher-frequency (1 h) surface circulation features from the HF radars in the GoKh along the northeastern Arabian Sea. Owing to the lack of any other current observations either on the surface or subsurface, the HF radars in this domain could provide a spatio-temporal variation of tidal currents for the first time quite efficiently. In this work, the low-frequency tidal constituents, Mf and MSf (fortnightly), are observed with significant amplitudes (Ray and Susanto 2016). Investigations will be carried out in the near future to unveil the dynamics of tidal mixing in the gulf and efforts will be made to identify the tidal fronts to relate those to the marine productivity utilizing some observational datasets and three-dimensional hydrodynamic models (Munandar et al. 2023). Further, there exist a few spatio-temporal gaps within the HF radar surface currents, which needs to be filled up considering both space and time, so that the gap filled higher-resolution datasets can be further utilized for the identification of tidal energy hotspots.

Acknowledgements The Science and Engineering Research Board (SERB) of the Department of Science and Technology (DST), Government of India, is acknowledged for financial support (Grant No: SRG/2023/000155). The author acknowledges the infrastructural as well as the financial (Young Faculty Incentive Fellowship) support from IIT Delhi, India. Also, the Coastal and Environmental Engineering (CEE) Group, National Institute of Ocean Technology (NIOT), India, is acknowledged for constant monitoring of the HF radars and Indian National Centre for Ocean Information Services (INCOIS), India, is acknowledged for making the data availability more efficient. The authors thank the anonymous reviewers, associate editor, and editor-in-chief for their constructive comments and suggestions.

Data availability The hourly surface currents from the HF radars (source: https://incois.gov.in/portal/datainfo/hfradar.jsp) and the hourly sea-level anomaly datasets from tide gauges (source: https://incois.gov.in/portal/datainfo/tidegauge.jsp) are available freely at request from INCOIS, India. The GHRSST sea surface temperature data are available at https://podaac.jpl.nasa.gov/GHRSST. The sea surface winds from Advanced Scatterometer (ASCAT) are available at http://apdrc.soest.hawaii.edu/datadoc/ascat.php. The sea surface salinity data are openly available at http://apdrc.soest.hawaii.edu/las/v6/constrain?var=2954. The ETOPO2 bathymetry dataset is openly available at http://apdrc.soest.hawaii.edu/las/v6/dataset?catitem=1296. The river discharge datasets are freely available at http://www.sage.wisc.edu/riverdata/index.php?qual=32.

Declarations

Conflict of interest The author declares no competing interests.

References

Ajai AB, Chauhan HB, Sarma KS, Bhattacharya S, Ashutosh S, Pandey CN, Thangaradjou T, Gnanppazham L, Selvam V, Nayak SR (2013) Mangrove inventory of India at community level. Natl Acad Sci Lett 36:67–77. https://doi.org/10.1007/s40009-012-0087-x

Arunraj KS, Jena BK, Suseentharan V, Rajkumar J (2018) Variability in eddy distribution associated with east India coastal current from high-frequency radar observations along southeast coast of India. J Geophys Res Ocean 123:9101–9118. https://doi.org/10.1029/2018JC014041

Bhatt S, Shah DG (2009) The mangrove diversity of Purna estuary, South Gujarat, India-tropical ecology. Trop Ecol 50:287–293

Chatterjee A, Shankar D, Shenoi SSC et al (2012) A new atlas of temperature and salinity for the North Indian Ocean. J Earth Syst Sci 121:559–593. https://doi.org/10.1007/s12040-012-0191-9

Chavanne C, Flament P, Carter G, Merrifield M, Luther D, Zaron E, Gurgel KW (2010) The surface expression of semidiurnal internal tides near a strong source at Hawaii. Part I: observations and numerical predictions. J Phys Oceanogr 40(6):1155–1179. https://doi.org/10.1175/2010JPO4222.1

Cook TM, Shay LK (2002) Surface M2 tidal currents along the North Carolina shelf observed with a high-frequency radar. J Geophys Res 107(C12):3222. https://doi.org/10.1029/2002JC001320

Cosoli S, Matjaz L, Vodopivec M, Malacic V (2013) Surface circulation in the Gulf of Trieste (northern Adriatic Sea) from radar, model, and ADCP comparisons. J Geophys Res Oceans 118(11):6183–6200. https://doi.org/10.1002/2013JC009261

Gough MK, Garfield N, McPhee-Shaw E (2010) An analysis of HF radar measured surface currents to determine tidal, wind-forced, and seasonal circulation in the Gulf of the Farallones, California United States. J Geophys Res 15:C04019. https://doi.org/10.1029/2009JC005644

Jena BK, Arunraj KS, Suseentharan V, Tushar K, Karthikeyan T (2019) Indian coastal ocean radar network. Curr Sci 116(3):372–378. https://doi.org/10.18520/cs/v116/i3/372-378

Jena BK, Arunraj KS, Suseentharan V, Ramana MV (2020) Surface circulation off the Andaman Islands from HF radar observations. Curr Sci 118(11):1139–1145. https://doi.org/10.18520/cs/v118/i11/1739-1745

Kosro PM (2005) On the spatial structure of coastal circulation off Newport, Oregon, during spring and summer 2001, in a region of varying shelf width. J Geophys Res 110:C10S06. https://doi.org/10.1029/2004JC002769

Kumar, J.S.; Balaji, R., 2016. Tidal power potential assessment along the Gulf of Kutch, Gujarat, India. In Proceedings of the Asian wave and tidal energy conference (AWTEC) 2016, Singapore

Kumar SS, Balaji R (2015) Effect of bottom friction on tidal hydrodynamics along Gulf of Khambhat, India. Estuar Coast Shelf Sci 154:129–136. https://doi.org/10.1016/j.ecss.2015.01.012

Kumar VS, Kumar KA (2010) Waves and currents in a tide-dominated location off Dahej, Gulf of Khambhat, India. Mar Geod 33(2):218–231. https://doi.org/10.1080/01490419.2010.492299

Mandal S, Sil S, Gangopadhyay A, Murty T, Swain D (2018a) On extracting high-frequency tidal variability from HF radar data in the northwestern Bay of Bengal. J Oper Oceanogr 11(2):65–81. https://doi.org/10.1080/1755876X.2018.1479571

Mandal S, Sil S, Shee A, Venkatesan R (2018b) Upper ocean and sub-surface variability in the Bay of Bengal during cyclone ROANU: a synergistic view using in-situ and satellite observations. Pure Appl Geophys 175:4605–4624. https://doi.org/10.1007/s00024-018-1932-8

Mandal S, Sil S, Pramanik S, Arunraj KS, Jena BK (2019) Characteristics and evolution of a coastal mesoscale eddy in the western Bay of Bengal monitored by high-frequency radars. Dyn Atmos Oceans 88:101107. https://doi.org/10.1016/j.dynatmoce.2019.101107

Mandal S, Sil S, Gangopadhyay A, Jena BK, Venkatesan R (2020a) On the nature of tidal asymmetry in the Gulf of Khambhat, Arabian Sea using HF radar surface currents. Estuar Coast Shelf Sci 232:106481. https://doi.org/10.1016/j.ecss.2019.106481

Mandal S, Sil S, Gangopadhyay A (2020b) Tide-current-eddy interaction: a seasonal study using high frequency radar observations along the western Bay of Bengal near 16 °N. Estuar Coast Shelf Sci 232:106523. https://doi.org/10.1016/j.ecss.2019.106523

Mandal S, Pramanik S, Sil S, Arunraj KS, Jena BK (2020c) Submesoscale circulation features along the Andhra Pradesh coast, Bay of Bengal: observations from HF radars. J Coast Res 89:132–138. https://doi.org/10.2112/SI89-022.1

Mandal S, Sil S, Gangopadhyay A, Jena BK, Venkatesan R, Gawarkiewicz G (2021) Seasonal and tidal variability of sur-face currents in the western Andaman Sea using HF radars and buoy observations during 2016–2017. IEEE Trans Geosci Remote Sens 59(9):7235–7244. https://doi.org/10.1109/TGRS.2020.3032885

Mandal S, Gangopadhyay A, Balaji R, Sil S (2022) Evolution of a sub-mesoscale eddy leeward of Andaman Islands from HF radars. IEEE Geosci Remote Sens Lett 19:1503804. https://doi.org/10.1109/LGRS.2022.3156288

Maas LRM, Van Haren JJM (1987) Observations on the vertical structure of tidal and inertial currents in the central North Sea. J Mar Res 45(2):293–318

Müller M, Cherniawsky JY, Foreman MGG, Von Storch J-S (2014) Seasonal variation of the M2 tide. Ocean Dyn 64:159–177. https://doi.org/10.1007/s10236-013-0679-0

Munandar B, Wirasatriya A, Sugianto DN, Susanto RD, Purwandana A, Kunarso (2023) Distinct mechanisms of chlorophyll-a blooms occur in the Northern Maluku Sea and Sulu Sill revealed by satellite data, 102, 101360. https://doi.org/10.1016/j.dynatmoce.2023.101360

Nayak SR, Sahai B (1985) Coastal morphology: a case study of the Gulf of Khambhat (Cambay). Int J Remote Sens 6(3–4):559–567. https://doi.org/10.1080/01431168508948478

Nayak RK, Shetye SR (2003) Tides in the Gulf of Khambhat, west coast of India. Estuar Coast Shelf Sci 57:249–254. https://doi.org/10.1016/S0272-7714(02)00349-9

Nayak RK, Salim M, Mitra D, Sridhar PN, Mohanty PC, Dadhwal VK (2015) Tidal and residual circulation in the Gulf of Khambhat and its surrounding on the west coast of India. J Indian Soc Remote Sens 43(1):151–162. https://doi.org/10.1007/s12524-014-0387-3

Paduan JD, Cook MS (1997) Mapping surface currents in Monterey Bay with CODAR type HF radar. Oceanogr. 10:49–52. https://doi.org/10.5670/oceanog.1997.21

Pawlowicz R, Beardsley B, Lentz S (2002) Classical tidal harmonic analysis including error estimates in MATLAB using T_TIDE. Comput Geosci 28(8):929–937. https://doi.org/10.1016/S0098-3004(02)00013-4

Prandle D (1982) The vertical structure of tidal currents. Geophys Astro Fluid 22(1–2):29–49. https://doi.org/10.1080/03091928208221735

Rao AD, Joshi M, Ravichandran M (2009) Observed low-salinity plume off Gulf of Khambhat, India, during post-monsoon period. Geophys Res Lett 36:L03605. https://doi.org/10.1029/2008GL036091

Ray RD, Susanto RD (2016) Tidal mixing signatures in the Indonesian seas from high-resolution sea surface temperature data. Geophys Res Lett 43(15):8115–8123. https://doi.org/10.1002/2016GL069485

Rosenfeld L, Shulman I, Cook M, Paduan J, Shulman L (2009) Methodology for a regional tidal model evaluation with application to central California. Deep Sea Res Part II Top Stud Oceanogr 56:199–219. https://doi.org/10.1016/j.dsr2.2008.08.007

Rubio A, Mader J, Corgnati L, Mantovani C, Griffa A, Novellino A, Quentin C, Wyatt L, Schulz-Stellenfleth J, Horstmann J, Lorente P, Zambianchi E, Hartnett M, Fernandes C, Zervakis V, Gorringe P, Melet A, Puillat I (2017) HF Radar Activity in European Coastal Seas: Next Steps toward a Pan-European HF Radar

Network. Front Mar Sci 4:8. https://doi.org/10.3389/fmars.2017.00008

Sil S, Dey S, Mandal S (2022) Seasonal circulation of Gulf of Khambhat, India using high frequency radars, OCEANS 2022-Chennai, Chennai, India, 1-5. https://doi.org/10.1109/OCEANSChennai45887.2022.9775249

Singh JK (2020) Structural characteristics of mangrove forest in different coastal habitats of Gulf of Khambhat arid region of Gujarat, west coast of India. Heliyon 6(8):e04685. https://doi.org/10.1016/j.heliyon.2020.e04685

Souza AJ, Simpson JH (1996) The modification of tidal ellipses by stratification in the Rhine ROFI. Cont Shelf Res 18:997–1007. https://doi.org/10.1016/0278-4343(95)00042-9

Subeesh MP, Unnikrishnan AS (2016) Observed internal tides and near-inertial waves on the continental shelf and slope off Jaigarh, central west coast of India. J Mar Syst 157:1–19. https://doi.org/10.1016/j.jmarsys.2015.12.005

Testut L, Unnikrishnan AS (2016) Improving modeling of tides on the continental shelf off the west coast of India. J Coast Res 32(1):105–115. https://doi.org/10.2112/JCOASTRES-D-14-00019.1

Turner JS (1973) Buoyancy Effects in Fluids. Cambridge University Press, New York

Unnikrishnan AS, Gouveia AD, Vethamony P, (1999a) Tidal regime in Gulf of Kutch, west coast of India, by 2D model. J. Waterway, Port, Coastal, Ocean Eng., 125 (6), 276–284. https://doi.org/10.1061/(ASCE)0733-950X(1999)125:6(276)

Unnikrishnan AS, Shetye SR, Michael GS (1999b) Tidal propagation in the Gulf of Khambhat, Bombay High and surrounding areas. Proc Indian Acad Sci (Earth Planet Sci), 108, 155–177. https://doi.org/10.1007/BF02842329

Visser AW, Souza AJ, Hessner K, Simpson JH (1994) The effect of stratification on tidal current profiles in a region of freshwater influence. Oceanol Acta 17:369–381